

Achievement of Diffusional Independence at Nanoscale Liquid – Liquid Interfaces within Arrays

Yang Liu,[†] Masniza Sairi,^{†,‡} Gregor Neusser,[§] Christine Kranz,[§] and Damien W. M. Arrigan^{*,†}

[†] Nanochemistry Research Institute, Department of Chemistry, Curtin University, GPO Box U1987, Perth, Western Australia 6845, Australia

[‡] Mechanisation and Automation Research Centre, Malaysian Agricultural Research and Development Institute (MARDI), P.O. Box 12301, 50774 Kuala Lumpur, Malaysia

[§] Institute of Analytical and Bioanalytical Chemistry, University of Ulm, Albert-Einstein-Allee 11, 89081 Ulm, Germany

ABSTRACT: In this work, independent radial diffusion at arrayed nanointerfaces between two immiscible electrolyte solutions (nanoITIES) was achieved. The arrays were formed at nanopores fabricated by focused ion beam milling of silicon nitride (SiN) membranes, enabling the reproducible and systematic design of five arrays with different ratios of pore center-to-center distance (r_c) to pore radius (r_a). Voltammetry across water – 1,6-dichlorohexane nanoITIES formed at these arrays was examined by the interfacial transfer of tetrapropylammonium ions. The diffusion-limited ion-transfer current increased with the ratio r_c/r_a , reaching a plateau for $r_c/r_a \geq 56$, which was equivalent to the theoretical current for radial diffusion to an array of independent nanoITIES. As a result, mass transport to the nanoITIES arrays was greatly enhanced due to the decreased overlap of diffusion zones at adjacent nanoITIES, allowing each interface in the array to behave independently. When the r_c/r_a ratio increased from 13 to 56, the analytical performance parameters of sensitivity and limit of detection were improved from $0.50 (\pm 0.02) \text{ A M}^{-1}$ to $0.76 (\pm 0.02) \text{ A M}^{-1}$ and from $0.101 (\pm 0.003) \mu\text{M}$ to $0.072 (\pm 0.002) \mu\text{M}$, respectively. These results provide an experimental basis for the design of arrayed nanointerfaces for electrochemical sensing.

INTRODUCTION

Electrochemistry at nanoscale interfaces, including electron transfer at nanoelectrodes and ion transfer across nanointerfaces between two immiscible electrolyte solutions (nanoITIES), has attracted considerable interest in many research fields, such as nanomaterial design for effective energy conversion devices and sensitivity improvement for miniaturized sensing platforms.¹⁻⁴ Nanoscale interfaces offer a number of advantages in electrochemical applications, such as decreased charging current, reduced ohmic drop and enhanced mass transport due to dominance of radial diffusion.⁵⁻⁷ Although single nanointerfaces have provided key insights into fundamental electrochemical processes,⁸⁻¹⁰ their low signal intensities and delicate fabrication procedures have limited their sensing applications. Therefore, arrays of nanointerfaces, in which a number of individual interfaces are arranged in parallel, were developed, to increase the electrochemical signals while maintaining the superior properties of the nanosystem.¹¹⁻¹³ However, the higher current obtained at nanointerface arrays may arise from an increase in the surface area rather than an improvement in analyte mass transport. Overlapped radial diffusion profiles between neighboring nanointerfaces may also result in strong analyte competition, thus decreasing the analytical sensitivity.^{14,15} Therefore, exploring the characteristics of arrayed nanointerfaces is essential for the improvement of their overall analytical performances, but requires in-depth understanding of analyte mass transport at the arrays.

In recent decades, mass transport behavior at microinterface arrays has been extensively studied. For example, a long-standing view was that microelectrode density in an array was optimal if $r_c > 12r_a$ (r_c : center-to-center distance; r_a : disc electrode radius).¹⁶ However, this was proven unsatisfactory in a simulation study of the diffusion process

at a regular array of microdisc interfaces.¹⁷ Fletcher and Horne proposed a more stringent design criterion, with $r_c > 20r_a$,¹⁸ which was further modified and experimentally verified by Davies *et al.*^{19,20} This design criterion provided important guidance to microelectrode array fabrication and triggered the progress of electrochemical applications.²¹⁻²³ Although the benefits which accrue from microinterfaces can be expected to be greater at nanointerfaces, the study of mass transport to nanoscale arrays is still at an early stage, and only simulation results that were subject to numerous approximations have been provided.²⁴ In addition to the issue of complex behaviors at nanointerfaces resulting from the comparable size of depletion layer and Debye length,²⁵ the difficulty in fabrication of nanoarrays with variable but well-controlled dimensions also a limitation. Recently, we reported the voltammetric behavior of cationic drug transfer across nanoITIES arrays in hexagonal arrangement ($r_c/r_a=20$),²⁶ which were prepared via electron beam lithography/reactive ion etching.²⁷ However, the experimental currents were lower than those expected for arrays of diffusionally-independent nanointerfaces,^{13,26-29} due to the overlap of diffusion zones between neighboring nanointerfaces.

In this work, focused ion beam (FIB) milling, a direct-write method enabling the reproducible and systematic control of nanoscale parameters, was employed to fabricate regular nanopore arrays of five designs ($r_c/r_a=13, 38, 56, 70$ and 82) in

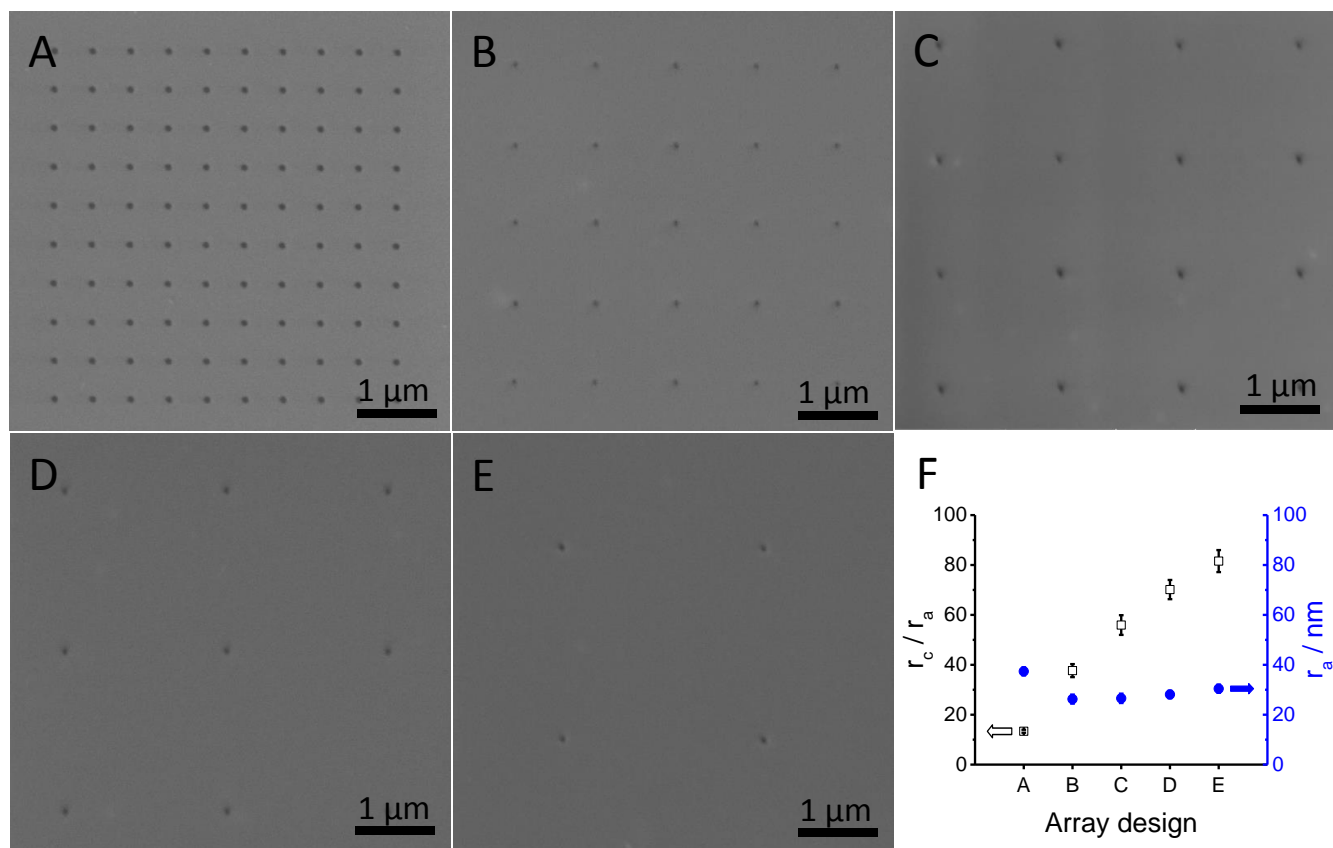


Figure 1. SEM images of nanopore arrays with r_c/r_a of 13 (A), 38 (B), 56 (C), 70 (D) and 82 (E). (F) The r_c/r_a (left Y axis, □) and r_a (right Y axis, ●) measured from the corresponding arrays in A-E. Error bars in (F) are ± 1 standard deviation, based on 9 pores.

silicon nitride (SiN) membranes. The voltammetric response of ion transfer across the nanoITIES arrays formed at these patterns was evaluated to determine the influence of array design. It was found that the ion-transfer limiting current increased to the theoretical current when r_c/r_a was higher than 56, in good agreement with previous simulation results.²⁴ From an analytical perspective, the sensitivity and limit of detection of the nanoITIES arrays were improved by tuning the nanointerface separation, which provides a promising approach for the development of nanosensing systems with high efficiency.

EXPERIMENTAL METHODS

The SiN membranes (DuraSiN film) with thickness of 50 nm, supported on rigid silicon frames (2.65 mm×2.65 mm×300 μm), were purchased from Electron Microscopy Sciences (Pennsylvania, USA). 10 × 10 array nanopores (radius r_a) with varying pore center-to-center separations (r_c) were fabricated with a DualBeam Helios Nanolab 600 FIB/SEM (FEI Company, Eindhoven, NL). The beam acceleration voltage was 30.0 kV and the beam current was 10 pA, giving a 12.8 nm ion beam probe size. After FIB milling, the arrays were imaged by SEM (acceleration voltage: 3.0 kV; through-the-lens detector) and the values of r_c and r_a were determined from the images.

All reagents were purchased from Sigma-Aldrich, and used as received. The electrolytes solutions were aqueous lithium chloride (LiCl) and bis(triphenylphosphoranylidene)ammonium tetrakis(4-chlorophenyl)borate (BTP-PATPBCl) in 1,6-dichlorohexane (1,6-DCH), both at 10 mM. The organic electrolyte salt was prepared as before.³⁰

Voltammetric experiments at the nanopore-supported nanoITIES arrays were performed with an Autolab PGSTAT 302N with ECD module (Metrohm, The Netherlands). A two-electrode cell with both electrodes serving as reference and counter electrode in their respective phases was housed in a Faraday cage. The nanoporous SiN membrane was affixed, via its silicon frame, to a borosilicate glass tube with silicone sealant. Approximately 200 μL of the organic phase electrolyte was added to the borosilicate glass tube, which was subsequently immersed in 6 mL of the aqueous phase solution. The electrochemical cell was as follows:



where x is the concentration of tetrapropylammonium chloride.

RESULTS AND DISCUSSION

FIB milling was used to fabricate regular nanopore arrays due to its high material removal efficiency and good dimensional controllability, which enables reproducible and systematic preparation of nanostructures.³¹ This direct-write technique provides an alternative approach^{32,33} to other nanofabrication methods based on high-energy particle beams, such as electron-beam lithography, which requires more complex and time-consuming procedures. Figure 1(A-E) shows the SEM images of the five nanopore square array designs with r_c/r_a of 13 (A), 38 (B), 56 (C), 70 (D) and 82 (E). Figure 1(F) summarizes the geometric characteristic of the arrays extracted from

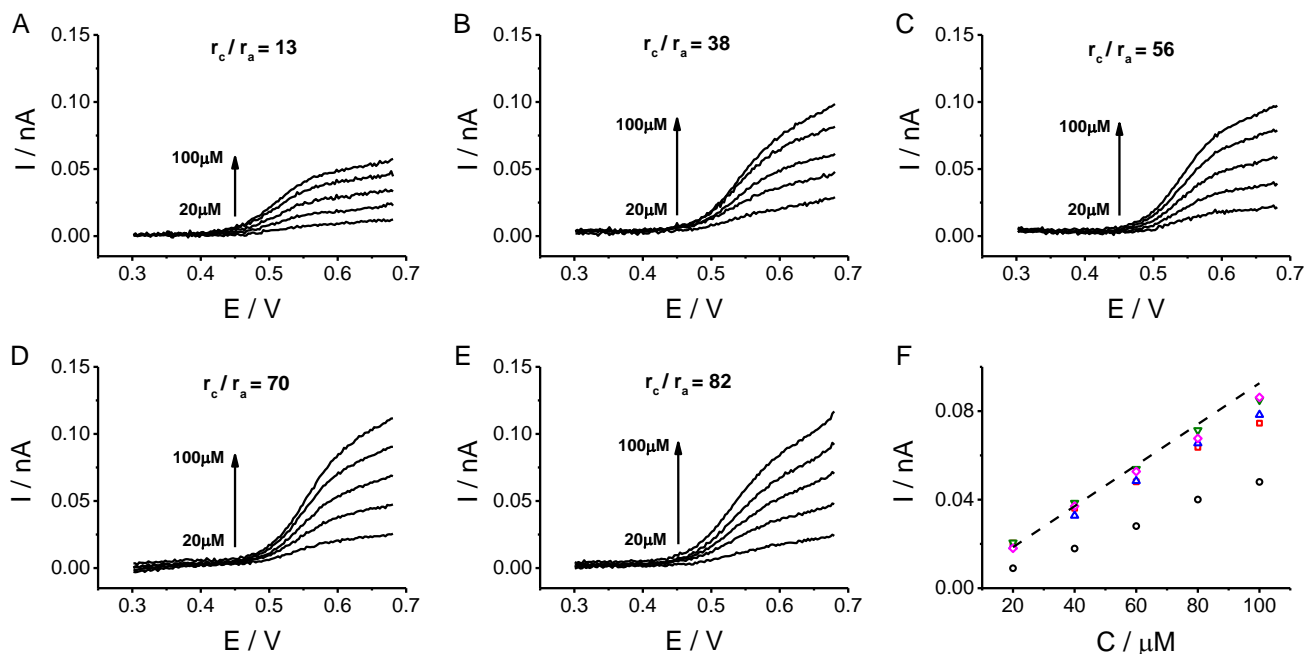


Figure 2. Background-subtracted voltammograms of 20, 40, 60, 80 and 100 μM TPrA⁺ transfer across the nanoITIES arrays with r_c/r_a of 13 (A), 38 (B), 56 (C), 70 (D) and 82 (E), scan rate: 5 mV/s. (F) Experimental calibration plots obtained from the nanoITIES arrays with r_c/r_a of 13 (○), 38 (□), 56 (△), 70 (▽) and 82 (◇). The black dashed line shows the theoretical calibration curve (Eq. (1)) based on the mean pore radius across the five arrays.

these images. It can be observed that nanopores with radii (r_a) ranging from 26 to 37 nm were successfully milled in SiN membranes (Figure 1F, right Y axis). In order to confirm the quality of the nanopore arrays, their properties, such as pore shape and size, were evaluated prior to each set of electrochemical experiments. Although the nanopores were not always perfectly round, the radii within each array, calculated by fitting a circle to the image of the nanopore, had a small dispersion, with relative standard deviations less than 7% in all cases. This was acceptable precision for practical experiments. Figure 1F (left Y axis) displays the determined r_c/r_a values, which were in the range 13-82. This provided the basis to investigate the effect of pore spacing on the electrochemical signals at nanoITIES arrays. All designs were 10×10 square arrays, so that the cross-sectional geometric area was constant and the key variable was the r_c/r_a value. For these square arrays, r_c was the distance between nanopores on the sides of the squares.

Electrochemical characterization of the arrays were implemented by monitoring the current response for tetrapropylammonium (TPrA⁺) transfer across the arrayed nanoITIES formed at the SiN nanopore membranes. Prior to the analyte transfer, cyclic voltammograms (CVs) of the background electrolyte solutions were recorded over a potential range sufficient to encompass TPrA⁺ transfer. The background-subtracted voltammograms (forward scan only) for five concentrations (20, 40, 60, 80 and 100 μ M) of TPrA⁺ at each of the nanoITIES array designs are shown in Figure 2(A-E). The analyte commenced transfer from aqueous phase to organic phase at 0.45 V, and the current increased steadily until a “sloping steady-state” current was reached in the diffusion-limited region, in good agreement with the electrochemical behaviors of nanoITIES arrays reported previously.^{28,29,32} In the absence of a definite steady-state current plateau, the currents recorded at 0.6 V, where an initial sloping steady-state current was reached, were determined as the experimental limiting currents for evaluation of the properties of the nanoITIES arrays.

The limiting current for TPrA⁺ transfer increased with concentration at the five nanoITIES array designs. Interestingly, the currents measured at the array with r_c/r_a of 13 (Figure 2A) were lower than those obtained with the other designs, illustrating the impact of the pore-to-pore separations on diffusion to the arrays. In order to compare the ion-transfer behaviors of the five nanoITIES arrays, calibration curves for TPrA⁺ at the five nanoITIES array designs were plotted (Figure 2F). Sairi *et al.* investigated TPrA⁺ transfer across single nanoITIES formed at a FIB-milled SiN membrane.³² The ion-transfer current results at this single nanoITIES was in excellent agreement with the theoretical current for an inlaid disc interface, which suggested that such FIB-milled nanopores enable the formation of inlaid nanointerfaces that are co-planar with the aqueous side of the SiN membrane. Since the same fabrication process was employed in this work, the nanoITIES behaves like an inlaid disk electrode and the theoretical limiting currents can be calculated with the Saito-Soos equation,^{16,34} modified to take into account the number of nanoITIES per array

$$I=4|z|FDc^b r_a N_p \quad (1)$$

where I is the limiting current, z , D and c^b are the charge, the diffusion coefficient and the bulk concentration of the transferring ion, respectively, F is Faraday’s constant (96485 C mol^{-1}), r_a is the individual interface radius and N_p is the number of pores used to form the nanoITIES array. In this work, $z = 1$, $D = 7.5 \times 10^{-10} \text{ m}^2 \text{ s}^{-1}$ ³⁵ and $N_p = 100$ were employed for all arrays. For indicative purposes, a theoretical calibration curve based on the mean pore radius, $r_a = 32 (\pm 5) \text{ nm}$, across all five nanoarrays was prepared (Figure 2F, dotted line). Comparing the slopes (analytical sensitivities) of the calibration curves, it can be seen that only half of the theoretical value was achieved when $r_c/r_a = 13$. This can be attributed to the strong overlap of diffusion zones at this low pore-to-pore separation; indeed, $r_c/r_a = 20$ was previously reported to produce overlapped diffusion zones at nanoITIES hexagonal arrays.^{27,29} However, the experimental results approached the theoretical average value as the r_c/r_a increased to 38, 56, 70 and 82, indicating that diffusion zone overlap is minimized and eventually eliminated as the pore-to-pore separation is increased. This opens up the possibility to achieve independent radial diffusion to nanointerfaces within an array. Although a previous simulation study showed that the steady-state current at nanoelectrode arrays was close to the theoretical current as the electrode center-to-center distance was increased to 60-times the radius,²⁴ the experimental observation of this effect is presented here for the first time (Figure 2).

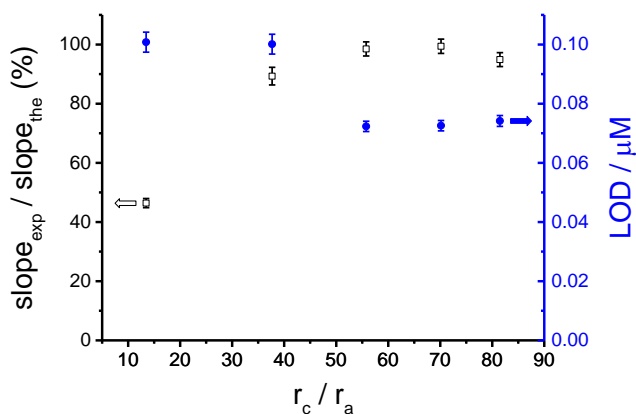


Figure 3. The effect of r_c/r_a (13, 38, 56, 70 and 82) on the experimental as a percentage of the theoretical slope (left Y axis, □) and the calculated limit of detection (right Y axis, ●) for TPrA⁺ transfer across the arrays of nanoITIES. Error bars are ± 1 standard deviation, based on the standard deviation of the slope.

Considering the variation of the pore radii across the array designs, which results in different theoretical currents for each array, but which are ignored by comparison to an average pore radius current (Figure 2F), individual array radii were used to evaluate the ratio of experimental to theoretical calibration curve slopes (Figure 3, left Y axis). The results show that the slope percentage increased from $46 \pm 2\%$ to $89 \pm 3\%$, with the increase of the r_c/r_a from 13 to 38, due to the enhanced ion flux arising from the convergent diffusion to the nanoITIES. When the r_c/r_a was increased to 56, $99 \pm 2\%$ of the theoretical current was achieved, which showed that independent radial diffusion occurred to each nanointerface in the array. These results were consistent with simulation data, which predicted that 97% of the theoretical current can be achieved at a 6×6 nanodisc array when $r_c/r_a = 60$.²⁴ Furthermore, at values of r_c/r_a larger than 56, the experimental-to-theoretical current slope plateaued at $95 \pm 2\%$, further supporting the occurrence of independent diffusion at each nanoITIES in the arrays.

Much larger pore-to-pore separations were required to eliminate diffusion zone overlap at nanoITIES arrays compared with that at micro-arrays, which may be attributed to the profound behaviors of mass transport at nanoscale.³⁶⁻³⁸ It has to be noted that the nanopore arrays investigated here are in a square arrangement and the r_c values were calculated based on the side lengths of squares, which means the real values of r_c/r_a are larger than the calculated ones due to the longer diagonal distance in a square. This factor may result in achievement of independent diffusion at an apparently lower r_c/r_a value than expected, but will have no impact on the trend of diffusion zone overlap at nanoarrays. Since FIB is a powerful tool for nanopatterning, the study of ion diffusion at nanoITIES arrays with different arrangements is the subject of further experiments.

From a chemical sensing perspective, the sensitivity of nanoarrays directly depended on the inverse of the interface radius, at fixed values of r_c/r_a .²⁹ However, the overlap of diffusion zones at adjacent nanoITIES limited the radial diffusion to each interface, thus decreasing the sensitivity of the entire array. In this work, the sensitivity (equivalent to Figure 3, left axis) for TPrA⁺ transfer at arrayed nanoITIES with the design of $r_c/r_a = 13$ was $0.50 (\pm 0.02) \text{ A M}^{-1}$, which increased to $0.76 (\pm 0.02) \text{ A M}^{-1}$ when independent radial diffusion was achieved at the array with $r_c/r_a = 56$. This can be attributed to the optimal utilization of each interface of the arrays. Besides sensitivity, limit of detection (LOD) is another important parameter of the analytical performances of nanosensing systems. Figure 3 (right Y axis) shows the calculated LOD (based on 3-times the standard deviation) for TPrA⁺ transfer across the nanoITIES arrays. It shows that the LOD was lowered from $0.101 (\pm 0.003) \mu\text{M}$ at the array design of $r_c/r_a = 13$ to $0.072 (\pm 0.002) \mu\text{M}$ at that of $r_c/r_a = 56$. It means that design of nanoITIES arrays with r_c/r_a of 56 is sufficient to improve the LOD, even with CV detection.

CONCLUSION

For the first time, independent radial diffusion was achieved at arrays of nanoITIES formed by nanopores in SiN membranes designed so that $r_c/r_a \geq 56$, which is in agreement with previously-reported simulation results for nanoelectrode arrays.²⁴ FIB milling was employed to fabricate five nanopore array designs with $r_c/r_a = 13, 38, 56, 70$ and 82 , and TPrA⁺ interfacial transfer was used to examine the impact on ion transfer behavior. It was experimentally observed that the overlapped diffusion zones at nanoarrays are much stronger than that at microarrays, which suggests a deeper impact of mass transport behavior at arrayed nanodevices. In addition, attractive analytical performances such as higher sensitivity and lower LOD were obtained at the nanoITIES arrays exhibiting independent radial diffusion, providing a basis for the development of nanoarray-based electrochemical sensors with high performance.

AUTHOR INFORMATION

Corresponding Author

* E-mail: d.arrigan@curtin.edu.au. Fax: +61892662300. Phone: +61892669735.

Notes

The authors declare no competing financial interest.

ACKNOWLEDGMENT

The authors thank the Australian Research Council (DP130102040), the Deutscher Akademischer Austausch Dienst (DAAD) (project 57060632), and the Joint Research Co-operation Scheme of the Australian Technology Network and the DAAD (travel grant) for funding. The Focused Ion Beam Centre UUlM (supported by FEI Company, Eindhoven, Netherlands, German Science Foundation (INST40/385-F1UG) and Struktur- und Innovationsfonds Baden-Württemberg) and the Curtin University Electron Microscope Facility (partially funded by the University and the State and Commonwealth Governments) are thanked for access to facilities.

REFERENCES

- (1) Zhang, Q. F.; Uchaker, E.; Candelaria, S. L.; Cao, G. Z. *Chem. Soc. Rev.* **2013**, *42*, 3127-3171.
- (2) Guo, S.; Wang, E. *Acc. Chem. Res.* **2011**, *44*, 491-500.
- (3) Arrigan, D. W. M.; Herzog, G.; Scanlon, M. D.; Strutwolf, J. In *Electroanalytical Chemistry : A Series of Advances*, Bard, A. J.; Zoski, C. G., Eds.; Taylor and Francis: Hoboken, 2013, pp 105-178.
- (4) Liu, S.; Li, Q.; Shao, Y. *Chem. Soc. Rev.* **2011**, *40*, 2236-2253.
- (5) Arrigan, D. W. M. *Analyst* **2004**, *129*, 1157.
- (6) Amemiya, S.; Wang, Y.; Mirkin, M. V. In *Specialist Periodical Reports - Electrochemistry*, Compton, R. G.; Wadhawan, J. D., Eds.; The Royal Society of Chemistry: Cambridge, 2013, p 44.
- (7) Oja, S. M.; Wood, M.; Zhang, B. *Anal. Chem.* **2013**, *85*, 473-486.
- (8) Chen, S. L.; Kucernak, A. *J. Phys. Chem. B* **2002**, *106*, 9396-9404.
- (9) Wang, Y.; Velmurugan, J.; Mirkin, M. V.; Rodgers, P. J.; Kim, J.; Amemiya, S. *Anal. Chem.* **2009**, *82*, 77-83.
- (10) Li, Q.; Xie, S.; Liang, Z.; Meng, X.; Liu, S.; Girault, H. H.; Shao, Y. *Angew. Chem. Int. Ed.* **2009**, *48*, 8010-8013.
- (11) Ongaro, M.; Ugo, P. *Anal. Bioanal. Chem.* **2013**, *405*, 3715-3729.
- (12) Hees, J.; Hoffmann, R.; Yang, N.; Nebel, C. E. *Chem. Eur. J.* **2013**, *19*, 11287-11292.
- (13) Scanlon, M. D.; Arrigan, D. W. M. *Electroanalysis* **2011**, *23*, 1023-1028.
- (14) Amatore, C.; Saveant, J. M.; Tessier, D. *J. Electroanal. Chem.* **1983**, *147*, 39-51.
- (15) Dawson, K.; O'Riordan, A. *Annu. Rev. Anal. Chem.* **2014**, *7*, 163-181.
- (16) Saito, Y. *Rev. Polarogr.* **1968**, *15*, 177-187.
- (17) Lee, H. J.; Beriet, C.; Ferrigno, R.; Girault, H. H. *J. Electroanal. Chem.* **2001**, *502*, 138-145.
- (18) Fletcher, S.; Horne, M. D. *Electrochem. Commun.* **1999**, *1*, 502-512.
- (19) Davies, T. J.; Compton, R. G. *J. Electroanal. Chem.* **2005**, *585*, 63-82.

- (20) Davies, T. J.; Ward-Jones, S.; Banks, C. E.; del Campo, J.; Mas, R.; Muñoz, F. X.; Compton, R. G. *J. Electroanal. Chem.* **2005**, *585*, 51-62.
- (21) Guo, J.; Lindner, E. *Anal. Chem.* **2009**, *81*, 130-138.
- (22) Tomčík, P. *Sensors* **2013**, *13*, 13659-13684.
- (23) Huang, X.-J.; O'Mahony, A. M.; Compton, R. G. *Small* **2009**, *5*, 776-788.
- (24) Godino, N.; Borrisé, X.; Muñoz, F. X.; del Campo, F. J.; Compton, R. G. *J. Phys. Chem. C* **2009**, *113*, 11119-11125.
- (25) Dickinson, E. J. F.; Compton, R. G. *J. Electroanal. Chem.* **2011**, *661*, 198-212.
- (26) Liu, Y.; Strutwolf, J.; Arrigan, D. W. M. *Anal. Chem.* **2015**, *87*, 4487-4494.
- (27) Scanlon, M. D.; Strutwolf, J.; Blake, A.; Iacopino, D.; Quinn, A. J.; Arrigan, D. W. M. *Anal. Chem.* **2010**, *82*, 6115-6123.
- (28) Sairi, M.; Strutwolf, J.; Mitchell, R. A.; Silvester, D. S.; Arrigan, D. W. M. *Electrochim. Acta* **2013**, *101*, 177-185.
- (29) Rimboud, M.; Hart, R. D.; Becker, T.; Arrigan, D. W. M. *Analyst* **2011**, *136*, 4674-4681.
- (30) Lee, H. J.; Beattie, P. D.; Seddon, B. J.; Osborne, M. D.; Girault, H. H. *J. Electroanal. Chem.* **1997**, *440*, 73-82.
- (31) Tseng, A. A. *Small* **2005**, *1*, 924-939.
- (32) Sairi, M.; Chen-Tan, N.; Neusser, G.; Kranz, C.; Arrigan, D. W. M. *ChemElectroChem* **2015**, *2*, 98-105.
- (33) Lanyon, Y. H.; De Marzi, G.; Watson, Y. E.; Quinn, A. J.; Gleeson, J. P.; Redmond, G.; Arrigan, D. W. M. *Anal. Chem.* **2007**, *79*, 3048-3055.
- (34) Soos, Z. G.; Lingane, P. J. *J. Phys. Chem.* **1964**, *68*, 3821-3828.
- (35) Langmaier, J.; Stejskalova, K.; Samec, Z. *J. Electroanal. Chem.* **2001**, *496*, 143-147.
- (36) Wahl, A.; Barry, S.; Dawson, K.; MacHale, J.; Quinn, A. J.; O'Riordan, A. *J. Electrochem. Soc.* **2013**, *161*, B3055-B3060.
- (37) Krapf, D.; Quinn, B. M.; Wu, M.-Y.; Zandbergen, H. W.; Dekker, C.; Lemay, S. G. *Nano Lett.* **2006**, *6*, 2531-2535.
- (38) Schmueser, I.; Walton, A. J.; Terry, J. G.; Woodvine, H. L.; Freeman, N. J.; Mount, A. R. *Faraday Discuss.* **2013**, *164*, 295.

Table of Contents artwork

